npj | flexible electronics

www.nature.com/npjflexelectron

ARTICLE OPEN

Check for updates

UV-laser-machined stretchable multi-modal sensor network for soft robot interaction

Jooyeun Ham[1], Amy Kyungwon Han[1,2], Mark R. Cutkosky[1] and Zhenan Bao[3]✉

Soft robotic hands can facilitate human–robot interaction by allowing robots to grasp a wide range of objects safely and gently. However, their performance has been hampered by a lack of suitable sensing systems. We present a flexible and stretchable multi-modal sensor network integrated with a soft robotic hand. The design of wired sensors on a flexible metalized film was embodied through a manufacturing approach that uses both UV laser metal ablation and plastic cutting simultaneously to create sensor electrode and stretchable conductive wires in a Kirigami pattern into a single network. We evaluated the interconnects and sensors by measuring an impedance change to each external stimulus and showed that are not substantially affected by stretching the network. With the sensor sheet wrapped around a soft robotic gripper, we demonstrated several interaction scenarios, including a warm burrito for food handling, and a warm baby doll for medical applications.

npj Flexible Electronics (2022)6:94 ; https://doi.org/10.1038/s41528-022-00225-0

INTRODUCTION

There have been tremendous advancements in the field of soft robotics in recent years. In particular, soft robotic hands have been demonstrated to grasp and even manipulate complex-shaped, fragile, or deformable objects, a perennial challenge for conventional rigid robotics[1,2]. Based on these capabilities, they have emerged as a promising solution for industrial, human interaction, and medical applications[3–5]. Despite their potential and recent progress, the majority of robots still do not perform dexterous activities with such hands due to a lack of sensing for feedback control[6–8]. Hence the development of sensors for soft robotic hands remains a critical step.

In an effort to mimic soft robotic hands with cutaneous sensing, and facilitate human–robot interaction, many solutions have been proposed[9–16]. However, in many cases, soft robotic sensors are primarily concerned with sensing the state of the robot itself (e.g., sensing bending angles or internal pressure). A smaller number[17,18–21] provide cutaneous sensing for information about interactions between the robot and objects or surfaces. In related work, researchers have developed stretchable sensors for mounting on human skin[22–27]. However, most of these are not aimed at sensing contact phenomena like the proximity to a grasped object or the temperature of its surface.

The integration of traditional sensors on soft robots or prosthetics introduces a mismatch in terms of their mechanical properties. Most conventional sensors are rigid, but the surfaces of soft robots need to stretch and are curved. Therefore, the sensors and networks require stretchable and flexible form factors to conform to and move with soft surfaces, without unwanted strain effects in the sensor signal. Despite recent advances in soft sensing networks, persistent challenges include the cost and complexity of fabrication, the need to customize for different applications, and the integration of sensors with processing. In addition to these requirements, applications like food handling and human interaction add the need to have sensors that are easily replaced (and ideally disposable) to avoid contamination.

To address these issues, the sensor network design and demonstration reported here have a low fabrication and integration complexity, consistent with the cost and ease of replacement required for disposables. This work shows how to utilize UV laser manufacturing techniques for the fabrication of stretchable multi-sensing arrays that address such issues for soft robotic and prosthetic applications. Although the elements of sensing network components—such as sensors[28–30] and conductive wires[31–33] fabricated by UV laser manufacturing—have been reported, in this paper, we present the design of a multi-modal sensor network as reported here, including a combination of multiple flexible sensors and wire bundles on stretchable kirigami networks. It enables one to fabricate multiple sensors and wires on a 50 × 50 mm^2 sensor network, with a cost of $0.005 (USD) for metalized plastic film, in 3 min. By varying beam parameters (power, frequency, duty cycle, speed), we patterned different features on each metal and plastic layer of flexible conductive film. Integration can be easily achieved by stretching the cut pattern to wrap it around surfaces of various shaped commercial soft robots. By modifying the pattern dimensions, it can be scaled and customized for different applications with differing dynamic ranges, spatial resolution, and sensing elements. As an example, we demonstrate three temperature and six proximity sensors on a 30 × 50 mm soft gripper inner surface aimed at the food preparation industry.

In the following sections, we describe the design of a flexible sensor network for one-step one-material fabrication and present characterization tests, which support the demonstration of the sensor network on a soft robotic hand for such tasks as grasping cool and warm objects (e.g., a burrito) or touching the forehead of a baby.

RESULTS

Multi-modal sensing soft robotic skin

The sensing approach described here is based on metalized PET (Polyethylene Terephthalate) film and patterned by UV laser ablation and cutting. The material is the same as commonly used

[1]Department of Mechanical Engineering, Stanford University, 450 Serra Mall, Stanford, CA 94305, USA. [2]Department of Mechanical Engineering, Seoul National University, 1 Gwanak-ro Gwanak-gu, Seoul 08826, Korea. [3]Department of Chemical Engineering, Stanford University, 443 Via Ortega, Stanford, CA 94305, USA. ✉email: zbao@stanford.edu

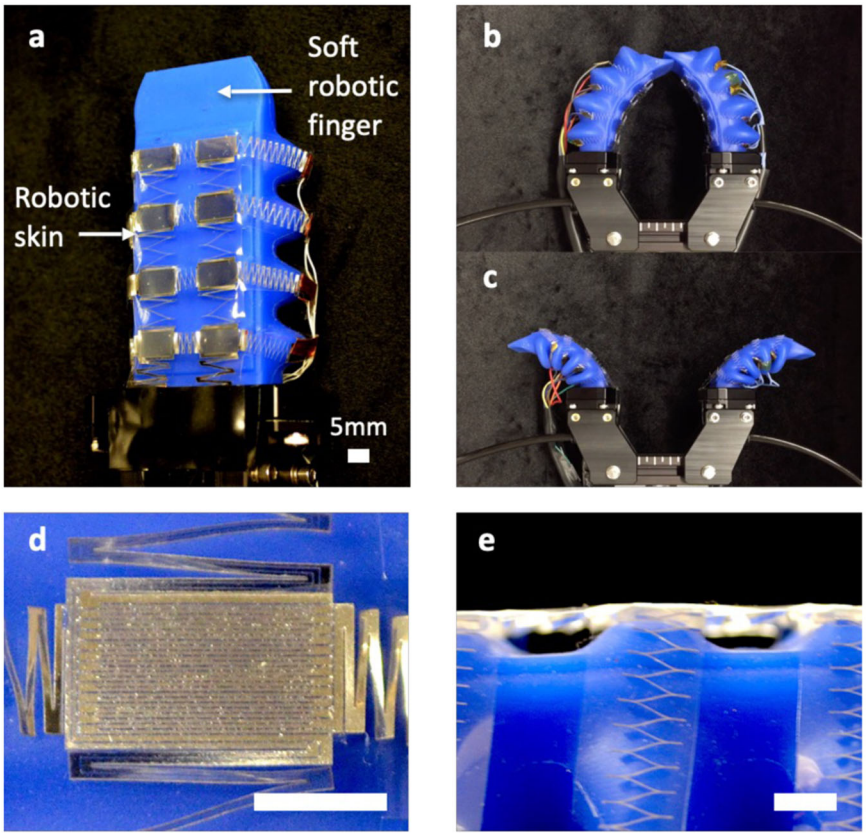

Fig. 1 Soft robotic hands with laser patterned Kirigami sensor network. To enhance the sensing ability of a soft robotic hand (Soft Robotics Inc.), a sensor network is embedded in a transparent silicone skin and stretched around it. **a** Image of the sensor network on a soft robotic finger. **b**, **c** Network accommodates large bending deflections, as shown in Supplementary Movie 1 and 2. **d** Magnified view of a thermal sensing unit (130 μm wide traces × 330 mm trace length) and stretchable interconnects (40–250 μm wide traces × 30 mm trace length) (**e**). Detail of interconnects embedded in a silicone skin.

for reflective window films and helium party balloons. By controlling the power of a UV laser, we can both create sensor patterns, ablating metal without damaging the plastic beneath, and then cut the film to create highly stretchable interconnects. We fabricated a robotic skin that consists of sensors connected by Kirigami wire traces, expanded and embedded in soft and stretchable silicone rubber (Fig. 1a). The skin is then stretched and wrapped around the soft fingers to keep it attached without wrinkles as the fingers flex and extend (Fig. 1b, c).

The example network, shown in Fig. 1a, consists of 4 temperature sensors and 4 proximity sensors with interconnects that provide 8 signals and 2 ground wires routed to the backs of the fingers. The sensors occupy discrete pads (Fig. 1d) that are flexible but not locally stretchable (maximum strain is 0.03, with impedance change of <0.01% for 60 cyclic tests.). Stretching occurs in the serpentine interconnects (Fig. 1e), which expand without substantially affecting sensor readings. The serpentine connectors can contain multiple conductive traces, which is useful for connecting multiple sensors to an analog-to-digital converter (ADC).

Material and methods

Ultraviolet lasers are a popular choice for cutting and patterning thin films of many materials, including plastics, metals, and composites[34]. We use a diode UV laser (2.66 W, 354.7 nm, DPSS Laser Inc.) for creating the sensors and cutting the film in a single setting (Fig. 2a). For the network reported here, we start with readily available sheets of 50 μm thick clear PET (Polyethylene Terephthalate) film with 50 nm thick reflective aluminum coating. We performed a parametric study over a range of laser settings to meet the following objectives: make traces as thin as possible, while also ensuring complete removal of metal from gaps between traces and preventing damage to the underlying film. We obtained the best patterning results with the following settings: a single pass at 100% of the rated power of 2.66 W, with a scan rate of 2000 mm s^{-1}, and a frequency of 60 kHz. Under these conditions, the minimum trace width is 30 μm, and the minimum gap width between traces is 20 μm. For different metals (e.g., copper) and film thicknesses, these settings and dimensions may change.

After patterning, we cut the film to create a Kirigami structure. After testing various cutting parameters to achieve clean cutting without carbonized edges that could produce shorting, we obtained the best results with the following settings: 7 times pass at 100% of the rated power of 2.66 W, with a scan rate of 150 mm s^{-1}, and frequency of 30 kHz. For different plastics (e.g., polyimide) and film thicknesses, these settings will change. With these settings, it is possible to cut strips as thin as 50 μm (removal width of 50 μm) with aluminum traces as thin as 30 μm wide (removal width of 20 μm). Figure 2b shows four sequential segments of a typical interconnect before expansion. The segments are 350 μm wide and separated by 50 μm gaps that cut through the PET layer to create parallel strips. On each strip are three parallel conductive traces with 20 μm gaps of ablated aluminum.

The fabrication process for creating the sensor network is fast and inexpensive. The film cost is less than $2 (USD) per square meter, and it takes about 3 min to fabricate 50 × 50 mm of sensing devices and interconnects in an unexpanded configuration.

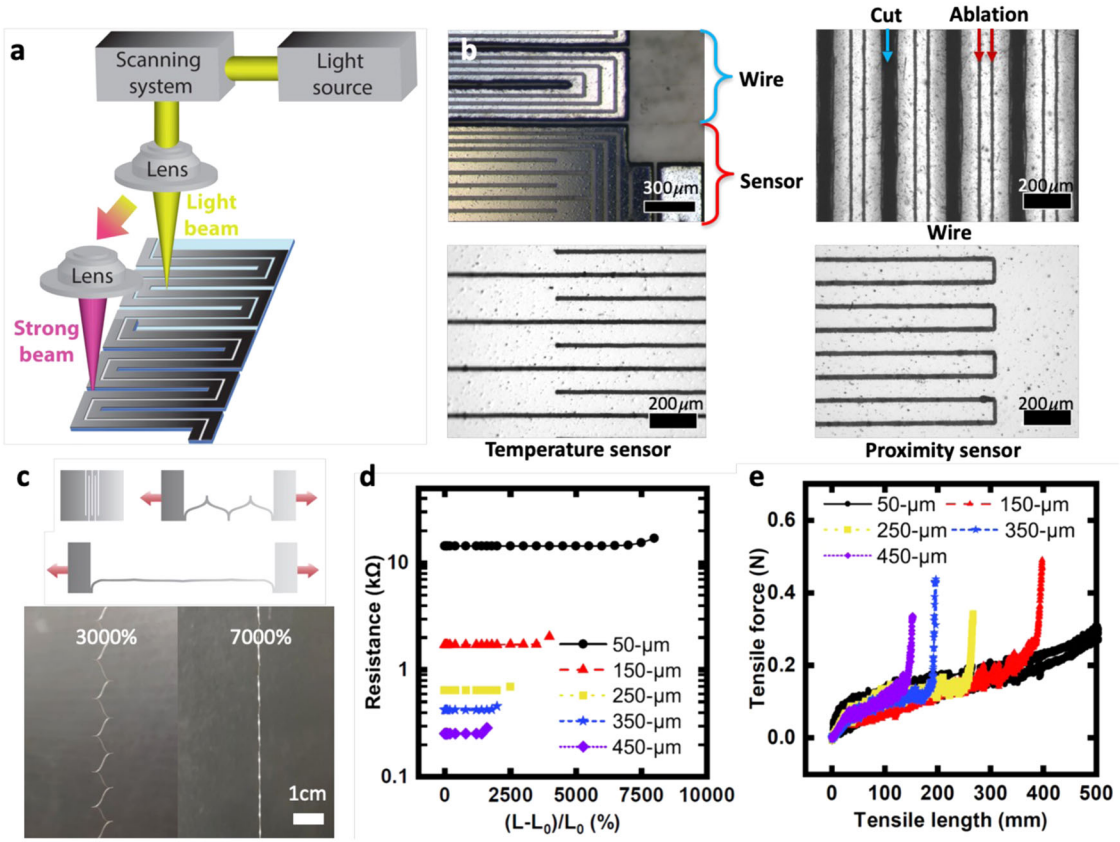

Fig. 2 Fabrication and characterization of the sensor network. a Illustration of laser ablation strategy, using low power to pattern the metal traces and higher power to cut the PET (Polyethylene Terephthalate) film. **b** Microscopic images of sensors and wires showing ablated aluminum sensors (red) and cut interconnect wires (cyan). Heavy black bars show a 200 μm length scale. **c** Diagrams and images showing Kirigami interconnect stretching. **d** Electrical and (**e**) mechanical properties of stretchable interconnects with different wire widths (traces fill the entire film width).

Adding a horizontal stage or feeding rollers to the laser would allow larger areas to be fabricated in a single setup.

Interconnects

Figure 2c shows schematically how the interconnects stretch, accompanied by images of interconnects stretched 30x and 70x. We note that the UV laser beam has a circular focal pattern that makes rounded edges when cutting serpentine patterns; this is beneficial for stress distribution.

For simplicity, we create sensors and interconnects in a tiled pattern with 10 × 10 mm regions interspersed with 10 × 10 mm interconnects. Thus, for a given 10 × 10 mm initial area of film, the design of the interconnect involves a tradeoff (Fig. 2d). In essence, patterns for thin traces (50 μm wide interconnect with 50 μm wide conductive trace) have higher resistance but can also stretch further before becoming taut, at which point the resistance starts to change. The trace resistance is given by

$$R = \frac{\rho}{A} \tag{1}$$

Initial resistances of the 50, 150, 250, 350, and 450 μm traces are 14.4, 3.4, 1.3, 0.85, and 0.51 kΩ (standard deviation of ±2 to 10%), respectively. The thinnest trace also shows the least change in resistance for stretching up to 70x because it undergoes the least material strain at the corners as the interconnect expands and straightens (see Fig. 2c). For the 50 μm traces, the change in resistance is approximately 1%, when the interconnect is stretched 70x; less than 17% for 80x of stretch. The resistance changes of the 150, 250, 350, and 450 μm wide Kirigami interconnects remain below 1% at strains of 3500%, 2000%, 1600%, and 1400%, respectively.

Figure 2e shows the force/extension behavior of the interconnects during stretching. All the interconnect patterns have relatively low stiffness (approximately 0.1 N per 0.4 m) until they become taut.

Proximity sensor

The proximity sensor is made by patterning two interdigitated comb electrodes (Fig. 3a). The fringe field generated between electrodes changes as a conductive object (e.g., a human finger or metal rod) approaches the sensor. The range and resolution of the sensor are tunable by the width and length of the pattern[35]:

$$\frac{c}{L} = \varepsilon\left[\frac{t}{h} + \frac{\pi\left(1 - 0.0543 \cdot \frac{W}{2h}\right)}{\ln\left(1 + \frac{2h}{W} + \sqrt{\frac{2h}{W}\left(\frac{2h}{W} + 2\right)}\right)} + 1.47\right] \tag{2}$$

where C is fringe capacitance, and ε is the dielectric constant. The width (W) of the electrode is adjustable, the thickness (t) is 50 nm, and the gap (h) is 20 μm, set by manufacturing limitations. If the comb electrodes are thinner and denser in designated sensor areas, a larger initial capacitance is obtained, which increases sensitivity (Fig. 3b). For the sensor network, a 130 μm wide comb pattern is chosen since it has less than 10% variation in line width due to manufacturing tolerances. Finite element simulation of the fringe capacitance for approaching objects was conducted using

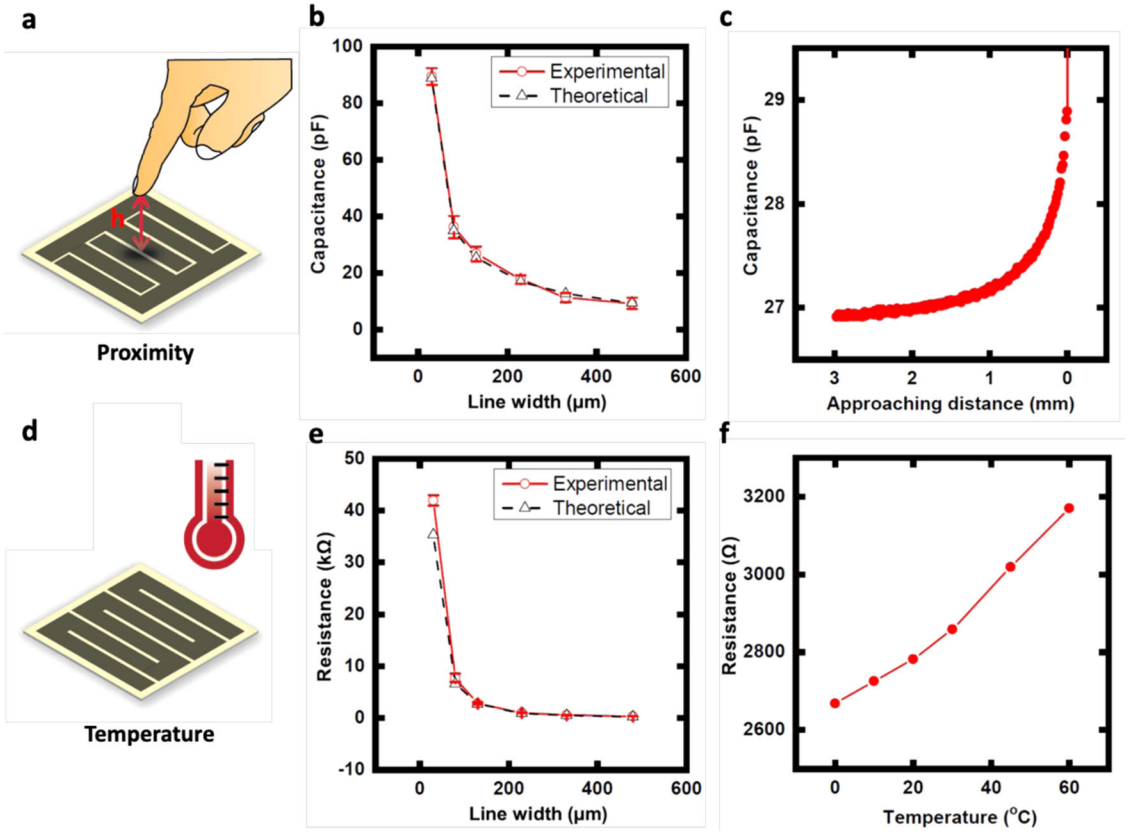

Fig. 3 Characteristics of proximity and temperature sensors. Theoretical solutions computed in COMSOL. a The proximity sensor is made of interdigitated comb patterns of aluminum on PET film. **b** Sensing resolution and range are tunable by initial capacitance, which depends on the number and dimensions of the traces; results match numerical simulations in COMSOL. **c** Distance from an approaching object (<3 mm) is measured by the change of fringing capacitance. **d** The temperature sensor is made of a meandering pattern with a 60,000:1 length: width ratio. **e** Temperature sensing resolution and range vary with initial resistance that depends on trace width and length; results match the theoretical calculation. **f** Temperature from 0 to 60 °C is measured by resistance, which changes approximately linearly with temperature.

COMSOL Multiphysics® v. 5.4. and showed that a 130 μm wide trace pattern with 20 μm gaps should have an initial capacitance of 1.85 pF for an object that is 3 mm distant. As the object draws closer, the capacitance increases by approximately 2 pF as the gap approaches zero.

Temperature sensor

The temperature sensor is made by patterning a meandering trace (Fig. 3d). Since aluminum is a thermoresistive metal, its resistance increases with temperature:

$$R = R_0[1 + \alpha(T - T_0)] \tag{3}$$

where α is the temperature coefficient of resistance (TCR) of the material used as the electrode, R_0 is the initial resistance at the reference temperature, and R is the resistance at temperature T. Range and resolution of the sensor are tunable by the width (W) and length (L) of the pattern:

$$\frac{dR}{dT} \sim \alpha\rho\frac{L}{Wt} \tag{4}$$

Sensors with a thinner and denser pattern have a larger initial resistance and higher sensitivity, as seen in Fig. 3e; theoretical and empirical results match within 7%. For the sensor network, a 130 μm wide meandering wire pattern is chosen from theoretical analysis. Given the resistance and change in resistance, a 130 μm wide with a 20 μm gap meandering electrode can detect 0.1 °C. When the fabricated sensor is placed in an oven, the resistance of 130 μm wide trace increases almost linearly with temperature over a range from 0 to 60 °C (Fig. 3f). Thus there is approximately 600 Ω resistance difference over 0 to 60 °C. Fitting a curve defined by Eq. (3) to the data results in a measured TCR of 3.14×10^{-3}, which is comparable to the reported TCR of aluminum (3.9×10^{-3})[36]; some difference is expected, given the very thin aluminum layer on PET film.

Design and integration of a sensor network

Figure 4 shows networks of temperature, and temperature and proximity sensors mounted on robotic fingertips (Soft Robotics Inc.). The interconnects are routed to the back of the hand and connected using conductive silver epoxy (Chemtronics CW2400) to wires and an analog to digital converter. The 5 × 10 mm sensors are mounted using soft, 1 mm thick VHB tape (3 M) to ridges on the insides of the fingers where contact generally occurs. These ridges undergo somewhat less strain than other parts of the fingers. Nonetheless, it is of interest to know whether the temperature sensors, which are also strain sensitive, are affected by opening and closing the fingers. Figures 4c, d show that the sensor readings change little (0.024% and 0.026%. respectively) over two successive opening and closing cycles. Supplementary Fig. 1 in the supplementary material shows that these changes remain constant over 30 opening and closing cycles.

Application—grasping warm and cool objects

Figure 5 shows how the contact sensors respond while acquiring, grasping, and moving cool and warm aluminum water bottles. The proximity sensor is used to detect an object approaching without touching it thereby avoiding abrasion or damage to the object.

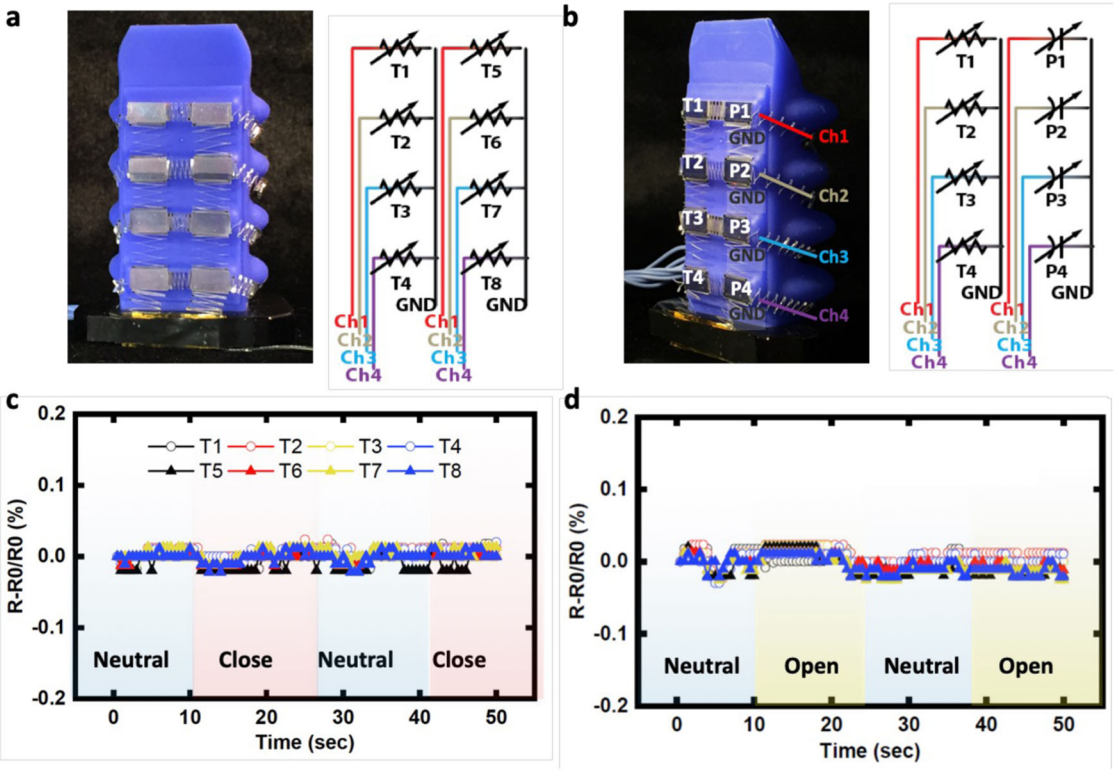

Fig. 4 Integration of actuation-independent sensor network on the soft robotic hand. a Sensor network integration on the soft robotic fingers (left). The network includes eight temperature sensors (T1–T8) with 130-μm-wide traces, connected by 350 μm cut interconnects with 1–5 traces (350 mm to 50 μm wide per electrical path). **b** Image and circuit diagram for the multimodal network of temperature and proximity sensors. Interconnects are as in (**a**). **c**, **d** Measured resistance change is small when closing and opening the fingers.

Approaching distance between a soft robot and an object supports to control the soft robotic actuation. When the proximity sensing indicates the contact of the soft gripper, it stops grasping and stays the position while temperature sensors measure the temperature. During the approach, the eight sensors all show a reading of (24.9 °C). The pair T2 and T6 are closest to the maximum bottle surface and initially have the largest contact areas, so they respond quickly. Subsequently, as the fingers continue to close, the other sensors that are in contact (T3, T7) approach the same temperature, while the proximal sensors (T4, T8) show a small increase in temperature. As a result, the measured temperature was 5.48 °C, as compared to the temperature (5.5 °C) measured with a thermometer immersed in the water. The results with a hot water bottle are similar. The measured temperature with the gripper is 55.2 °C, while the actual temperature is 55.7 °C.

Figure 6 illustrates the degree of repeatability to be expected for contact temperature and proximity sensors over multiple actuation cycles. The figures show the results as the finger contacts and conforms six times to a glass jar filled with warm water. While the finger contacts the jar, the strain on the robotic finger surface is 4.3% (71% of the maximum strain). To process data and report a temperature measurement, we converted measured resistance to temperature by using Eq. (3). The temperature of the object is provided by the temperature from a contact, which could be provided by proximity sensors on the network. Sensors P1 and P2, and corresponding temperature sensors T1 and T2, make contact with the jar and therefore show a much larger response than the other sensors. The measured temperature from the network is 38 °C, which is close to the water temperature, 39 °C.

The previous results suggest an application involving prepared food handling. To examine this application further, we use the sensor network to grasp a warm or cool burrito wrapped in foil. In this application, the proximity sensors are useful to ensure firm contact without excessive pressure, and the temperature sensors are useful to monitor the temperature. Because the burrito is wrapped in foil, an optical thermometer does not give a reliable temperature reading. Infrared (IR) thermometry has routinely been used in robotics to detect the temperature of a target object[37]. However, IR thermometer detection is dependent on the emissivity of the material[38]; for example, the emissivity is 1.2 for aluminum and only 0.1 for water. As shown in Supplementary Movie 3, the temperatures measured by an IR thermometer are not reliable since the measured temperatures at the outer and inner surfaces of the burrito are different. Direct contact temperature sensing can be a more reliable alternative in such applications.

Figure 7 shows the results of the burrito-handling task. The contact is primarily at the distal sensors, P1, and to a lesser extent, P2. As the first sensors make contact, we stop increasing the pressure to avoid crushing the burrito; hence the proximity signals remain constant. The temperature sensors show a similar trend. The measured temperature is 38.6 °C, which is close to the burrito temperature, 39.1 °C.

Application for human–robot interaction

The combination of proximity and temperature sensing is particularly useful for soft robot–human contact, allowing the robot to make gentle contact and allowing it to distinguish between living and nonliving surfaces or even to check for an elevated temperature. As a demonstration, Fig. 8 and Supplementary Movie 4 presents results for contacting the forehead of a doll. The forehead has been warmed to a temperature of 37.5 °C, measured by an IR thermometer. In this demonstration, the thermal contact sensors estimate the temperature as 36.8 °C

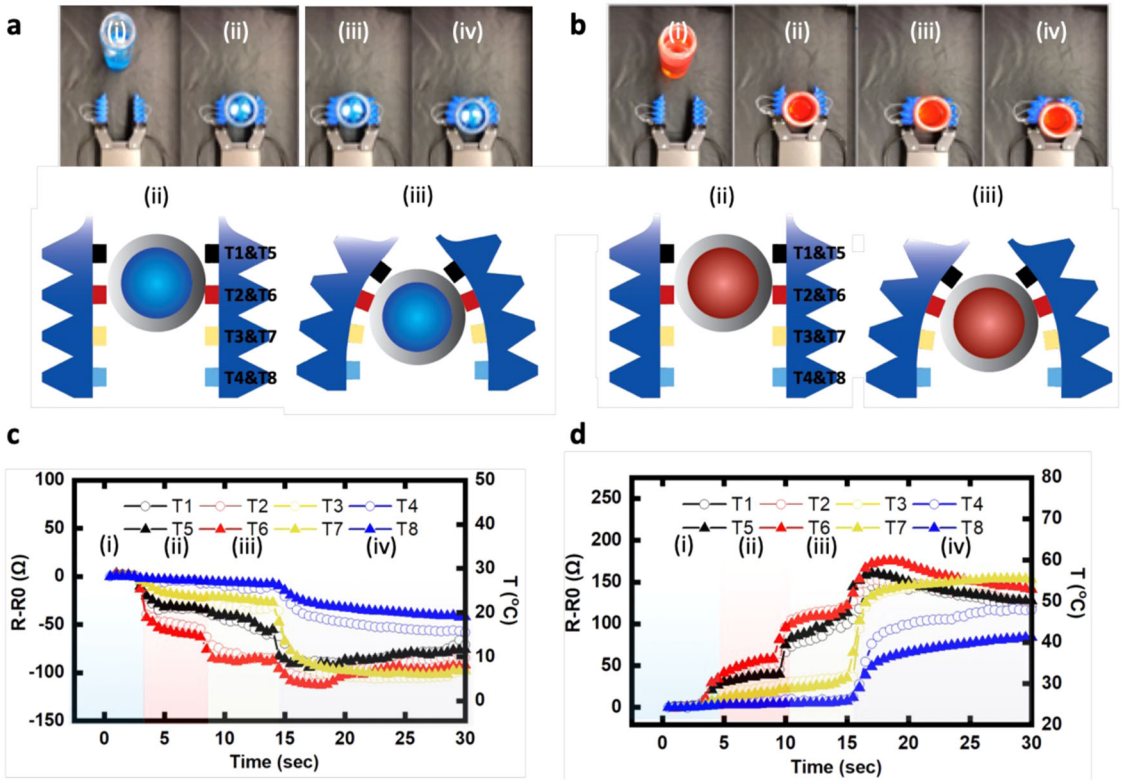

Fig. 5 Contact temperature sensing for cool and warm objects. (**a**) Images of (i) approaching, (ii) touching, (iii) grasping, and (iv) carrying a cool (5.5 °C) aluminum bottle filled with water. Diagrams (ii) and (iii) show which sensors are in contact for the corresponding phases. (c) shows the corresponding sensor readings. (**b**, **d**) show the same sequence as (**a**, **c**) but with a hot water bottle (55.7 °C).

(Fig. 8b). In this demonstration, proximity sensors are again used to control the finger to maintain a constant light pressure of approximately 1kPa after initial contact is detected.

DISCUSSION

Using metalized plastic film that is patterned and cut using a UV laser, it is possible to create a stretchable network of sensors at low cost. In contrast to most previous works, the design uses a single processing step so that sensor networks are created in minutes.

The laser can achieve traces of 130 µm width, separated by gaps of 20 µm. The traces can be designed as piezoresistive elements, e.g., for temperature or strain sensing, or as capacitive elements, e.g., for proximity and contact sensing. Cuts in the plastic film make it possible to create expandable interconnects in a Kirigami pattern so that a tiled array of 5 × 10 mm sensors expands to cover an area of 140 × 330 mm on the surface of a soft robot arm or hand. Once expanded, the network is embedded in a stretchable silicone rubber skin for protection. When mounted on soft pneumatic fingers, the sensors are not affected by the flexing of the fingers.

Motivating applications for the sensor network include food handling and human–robot interaction with soft robotic devices. In both cases, proximity sensing is useful to maintain gentle contact, while temperature sensors can distinguish between warm or cold food and between an elevated or normal skin temperature.

Future extensions include additional sensor types; for example, strain gages fabricated in situ for proprioceptive sensing and fringe-field sensors using a microstructured dielectric for combined proximity and pressure sensing. The addition of an *XY* stage or feed rolls for the film would allow the laser to pattern and cut much larger areas. For example, an array of 10 × 20 sensors and interconnects, initially occupying 155 × 200 mm in the unexpanded state, could be expanded to cover 520 × 1640 mm of the surface of a soft robot arm.

METHODS

Fabrication of the sensor network

Fabrication was conducted on a metalized PET film (Thickness of 50 µm, from McMaster) with an aluminum thickness of 0.05 µm.

The samples were cut into 50 × 50 mm^2 pieces, cleaned by IPA (Isopropyl Alcohol), and dried. Then the film was temporarily fixed on a glass slide with a drop of water, which produces a surface tension between the film and the glass slide. The prepared sample is placed on the stage of a UV laser machine.

UV laser machining was conducted by using a quasi-CW DPSS UV laser (DPSS Lasers Inc., Series 3500), with a calibrated power of 2.66 W on stage with 355 nm wavelength. The maximum power is varied by changing the driving current, which can be programmed easily through the customized software. It is driven by the laser beam from a laser diode to a built-in galvanometric beam scanning system.

The sample was mounted on the fixed stage of the *Z*-axis translator to adjust the focal point on the sample. Each pattern file for metal ablation and plastic cutting was prepared individually. The patterns of the sensor electrodes and the Kirigami wires were designed by a computer-aided design software (Auto CAD, Abode). The parameters of the laser beam's power, scan rate, scan pass, and frequency were set by computer-aided laser marking software (WinLaser) for each pattern. In the marking software, the UV laser beam condition was set at 100% power, 30 kHz, 7 time passes, 100 mm s^{-1} for cutting plastic of Kirigami wires and 100%, 60 kHz, single-pass, 2000 mm s^{-1} for ablating metal to pattern electrodes.

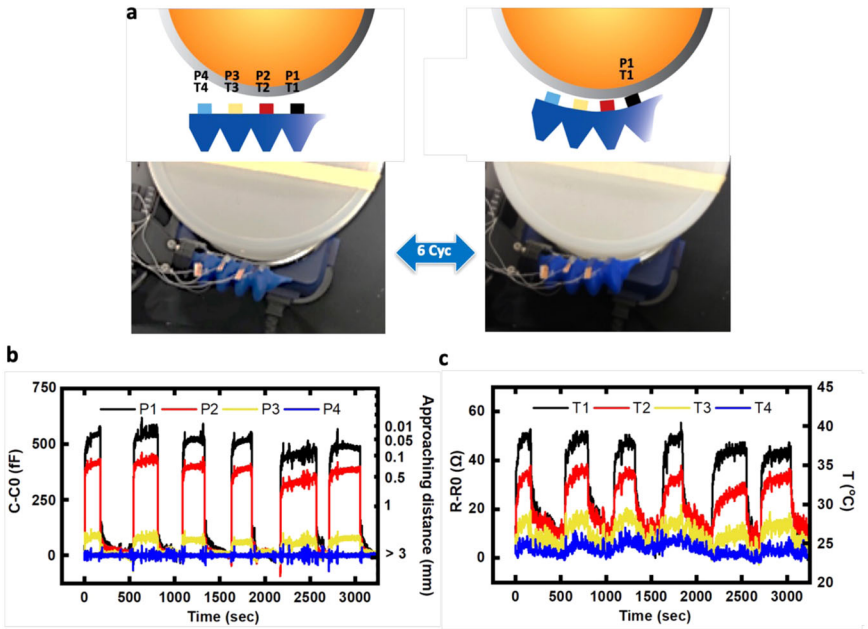

Fig. 6 Repeatability test of the sensor network. a Schematics and images of a finger with temperature (T1–T4) and proximity (P1–P4) sensors for six cycles of contact and finger actuation. The target object is a cylindrical jar filled with 38.0 °C water. **b** Proximity distribution measurement and (c) Temperature distribution measurement over the six actuation cycles.

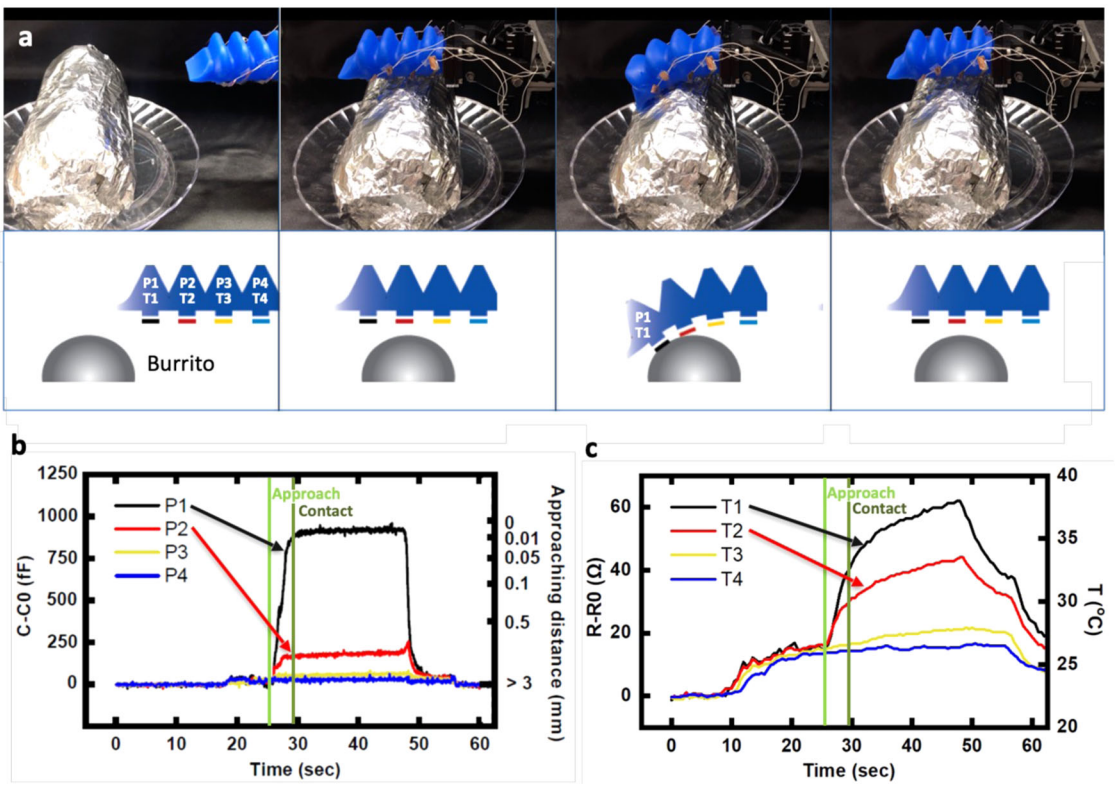

Fig. 7 Food handling demonstration using proximity and temperature sensing. a Images from left to right show the finger approaching, contacting, conforming to, and releasing from a foil-wrapped burrito. Plots (**b**, **c**) show the corresponding proximity and temperature readings. The contact is primarily at P1 and T1, with partial contact at P2 and T2. After initial contact is detected, the pressure is held constant. Robotic actuation and sensing are done simultaneously. The sequence is shown in Supplementary Movie 3.

The sensor network was fabricated in approximately 3 min. The patterned stretchable and flexible sensor network was released from the glass slide by applying more water.

Characterization of the sensors and sensor network

After the fabrication, optical microscopic images were obtained (Hitachi SU8020). The conductivity and the capacitance of the

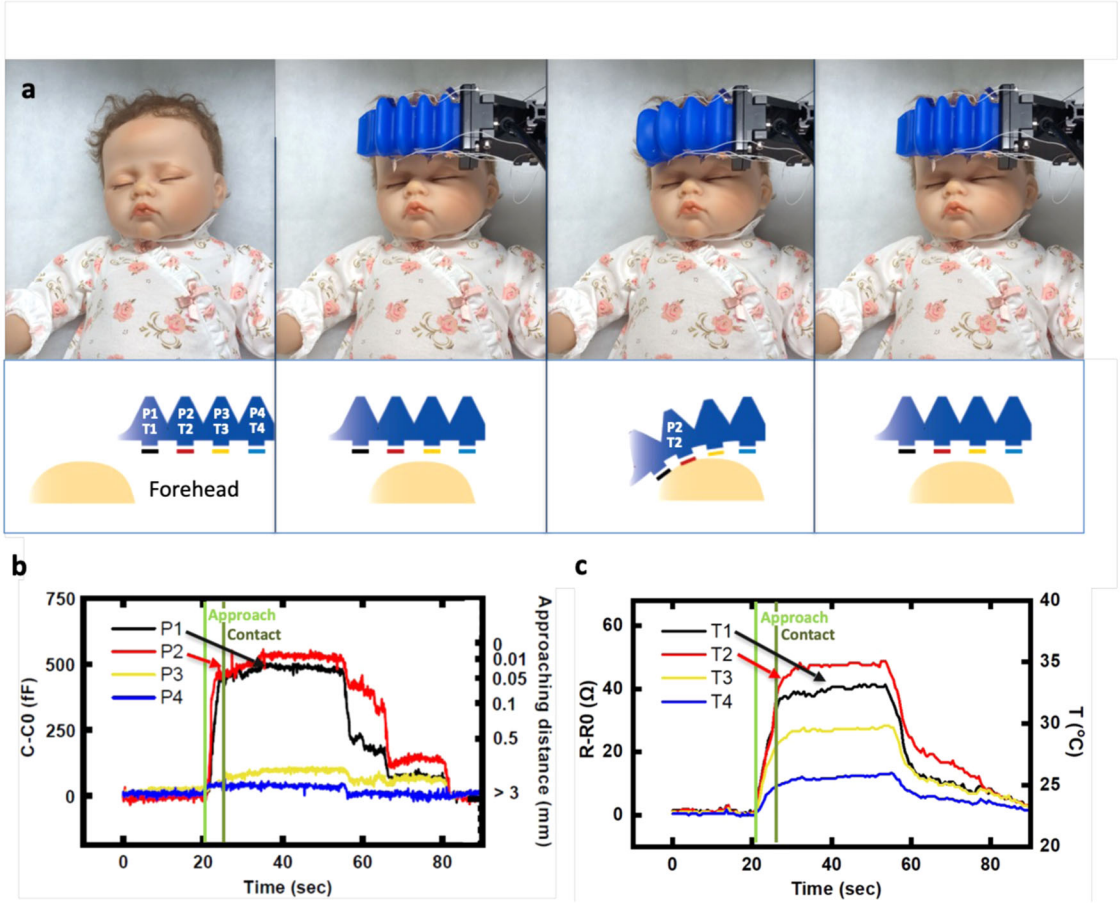

Fig. 8 Demonstration of soft robot–human interaction. a Images of a soft finger approaching and gently touching the forehead of a doll. Schematic of corresponding sensor contacts below. **b**, **c** Plots of corresponding proximity and temperature signals (calibrated data on the right vertical axis). The doll's forehead has been warmed to an elevated temperature of 37.5 °C, measured by an IR thermometer. Contact occurs primarily at sensor locations 1 and 2. Robotic actuation and sensing are done simultaneously. The sequence is shown in Supplementary Movie 4.

sensor and wires were analyzed by LCR meter (E4980A Precision LCR Meter, Keysight Technologies) and voltage-current source meter (Keithley 4200, Tektronix). The electrical connection to each wire was made by conductive silver epoxy (CW2400, Chemtronics) and thin jumper wires.

The temperature was controlled by an oven, while the impedance was measured by the Keithley meter. The distance between an approaching object and the sensor is controlled by a motorized vertical translator. The stretchability of the wire is measured using the LCR meter and a motorized horizontal translator (Instron 5565, Instron), which increases the elongation while measuring stress on the sample.

Integration of the sensor network on the soft robotic finger

To integrate the sensor network on the soft robotic finger, the flexible, but not stretchable, sensors were placed on a comparatively stiff part of the fingers using 3 M VHB double-sided tape. The final step is to embed the expanded network in a soft and stretchable skin. We use PDMS (Sylgard 184) cast to a thickness of 58 μm for demonstration. Lower stiffness and more stretchable silicone such as Ecoflex 00-10 can be used for applications that require more stretch.

To read multiple resistive sensors with an analog to digital conversion, channel wire and ground wire from each sensor were connected to the pins of a microcontroller (Adafruit Industries, Arduino MEGA). For capacitive signals, an evaluation board (Analog Devices, AD7147) was used. The resistive sensor readout was recorded at 2 Hz and capacitive sensor readout at 25 kHz.

After checking the impedance readout, we actuated the soft robotic finger, by supplying compressed air (up to 11 psi) for closing and vacuum for the extension.

DATA AVAILABILITY

All relevant data that support the findings of this study are available from authors upon reasonable request.

Received: 13 May 2022; Accepted: 1 November 2022;
Published online: 18 November 2022

REFERENCES

1. Shintake, J., Cacucciolo, V., Floreano, D. & Shea, H. Soft Robotic Grippers. *Adv. Mater.* **30**, 1707035 (2018).
2. Ilievski, F., Mazzeo, A. D., Shepherd, R. F., Chen, X. & Whitesides, G. M. Soft robotics for chemists. *Angew. Chem.* **123**, 1930–1935 (2011).
3. El-Atab, N. et al. Soft actuators for soft robotic applications: a review. *Adv. Intell. Syst.* **2**, 2000128 (2020).
4. Guo, J. et al. Design and fabrication of a pneumatic soft robotic gripper for delicate surgical manipulation. In: *IEEE International Conference on Mechatronics and Automation (ICMA)*, 1069–1074 (IEEE, 2017).
5. Park, Y. L. et al. Design and control of a bio-inspired soft wearable robotic device for ankle-foot rehabilitation. *Bioinspir. Biomim.* **9**, 016007 (2014).

6. Terryn, S. et al. Self-healing soft pneumatic robots. *Sci. Robot.* **2**, eaan4268 (2017).
7. Brown, E. et al. Universal robotic gripper based on the jamming of granular material. *Proc. Natl Acad. Sci. USA* **107**, 18809–18814 (2010).
8. Bartlett, N. W. et al. A 3D-printed, functionally graded soft robot powered by combustion. *Science* **349**, 161–165 (2015).
9. Kramer, Rebecca K. Soft electronics for soft robotics. *Micro- and Nanotechnology Sensors, Systems, and Applications VII*. Vol. 9467 (eds George, T., Dutta, A. K. & Saif Islam, M.) (SPIE, 2015).
10. Lu, N. & Kim, D. H. Flexible and stretchable electronics paving the way for soft robotics. *Soft Robot.* **1**, 53–62 (2014).
11. Case, J. C., Yuen, M. C., Jacobs, J. & Kramer-Bottiglio, R. Robotic skins that learn to control passive structures. *IEEE Robot. Autom. Lett.* **4**, 2485–2492 (2019).
12. Yamaguchi, A., Takemura, K., Yokota, S. & Edamura, K. A robot hand using electro-conjugate fluid. *Sens. Actuators A: Phys.* **170**, 139–146 (2011).
13. Yuen, M. C. S., Lear, T. R., Tonoyan, H., Telleria, M. & Kramer-Bottiglio, R. Toward closed-loop control of pneumatic grippers during pack-and-deploy operations. *IEEE Robot. Autom. Lett.* **3**, 1402–1409 (2018).
14. Ho, V. & Hirai, S. Design and analysis of a soft-fingered hand with contact feedback. *IEEE Robot. Autom. Lett.* **2**, 491–498 (2017).
15. Wall, Vincent et al. A method for sensorizing soft actuators and its application to the RBO hand 2. In: *IEEE International Conference on Robotics and Automation (ICRA)* 4965–4970 (IEEE, 2017).
16. Morrow, J. et al. Improving Soft Pneumatic Actuator fingers through integration of soft sensors, position and force control, and rigid fingernails. In: *Proc. IEEE International Conference on Robotics and Automation* 5024–5031 (IEEE, 2016).
17. Chin, L. et al. A simple electric soft robotic gripper with high-deformation haptic feedback. In: *IEEE International Conference on Robotics and Automation (ICRA)* 4965-4970 (IEEE, 2019).
18. Truby, R. L., Katzschmann, R. K., Lewis, J. A. & Rus, D. Soft robotic fingers with embedded ionogel sensors and discrete actuation modes for somatosensitive manipulation. *2019 IEEE International Conference on Soft Robotics* 322–329 (IEEE, 2019).
19. Zhao, H., O'Brien, K., Li, S. & Shepherd, R. F. Optoelectronically innervated soft prosthetic hand via stretchable optical waveguides. *Science Robotics* **1**, eaai7529 (2016).
20. Hellebrekers, T., Ozutemiz, K. B., Yin, J. & Majidi, C. Liquid metal-microelectronics integration for a sensorized soft robot skin. In: *IEEE International Conference on Intelligent Robots and Systems* 5924–5929 (IEEE, 2018).
21. Kim, J. et al. Stretchable silicon nanoribbon electronics for skin prosthesis. *Nat. Commun.* **5**, 5747 (2014).
22. Case, J., Yuen, M., Mohammed, M. & Kramer, R. In *Stretchable Bioelectronics for Medical Devices and Systems* (ed. Rogers, J. A.) 173–191 (Springer International Publishing, 2016).
23. Lopes, P. A. et al. Soft bioelectronic stickers: selection and evaluation of skin-interfacing electrodes. *Adv. Healthc. Mater.* **8**, 1900234 (2019).
24. Son, D. et al. Multifunctional wearable devices for diagnosis and therapy of movement disorders. *Nat. Nanotechnol.* **9**, 397–404 (2014).
25. Kim, D. H. et al. Epidermal electronics. *Science* **333**, 838–843 (2011).
26. Sim, K. et al. Metal oxide semiconductor nanomembrane–based soft unnoticeable multifunctional electronics for wearable human-machine interfaces. *Sci. Adv.* **5**, eaav9653 (2019).
27. Hua, Q. et al. Skin-inspired highly stretchable and conformable matrix networks for multifunctional sensing. *Nat. Commun.* **9**, 1–11 (2018).
28. Kothuru, A. et al. Laser-induced flexible electronics (LIFE) for resistive, capacitive and electrochemical sensing applications. *IEEE Sens. J.* **20**, 7392–7399 (2020).
29. Qin, R. et al. Flexible fabrication of flexible electronics: a general laser ablation strategy for robust large-area copper-based electronics. *Adv. Electron. Mater.* **5**, 1900365 (2019).
30. Bian, J. et al. Laser transfer, printing, and assembly techniques for flexible electronics. *Adv. Electron. Mater.* **5**, 1800900 (2019).
31. Yao, S. et al. Nanomaterial-enabled flexible and stretchable sensing systems: processing, integration, and applications. *Adv. Mater.* **32**, 1902343 (2020).
32. Won, P. et al. Stretchable and transparent kirigami conductor of nanowire percolation network for electronic skin applications. *Nano Lett.* **19**, 6087–6096 (2019).
33. Marchiori, B., Delattre, R., Hannah, S., Blayac, S. & Ramuz, M. Laser-patterned metallic interconnections for all stretchable organic electrochemical transistors. *Sci. Rep.* **8**, 8477 (2018).
34. Mishra, S. & Yadava, V. Laser beam micromachining (LBMM)—a review. *Opt. Lasers Eng.* **73**, 89–122 (2015).
35. Pucknell, D. A., & Eshraghian, K. *Basic VLSI Design Principles & Applications* (Prentice-Hall,1985).
36. Serway, R. A., & Jewett, J. W. *Principles of Physics* Vol. 1 (Saunders College Publishers, 1998).
37. Kim, J. H. & Lattimer, B. Y. Real-time probabilistic classification of fire and smoke using thermal imagery for intelligent firefighting robot. *Fire Saf. J.* **72**, 40–49 (2015).
38. Brewster, M. Q. *Thermal Radiative Transfer and Properties* (John Wiley & Sons, 1992).

ACKNOWLEDGEMENTS

The authors thank the members of Zhenan Bao Research Group and BDML at Stanford University. This study was supported by Beijing Institute of Collaborative Innovation (BICI). J.H. and A.K.H. were partially supported by the Samsung Scholarship.

AUTHOR CONTRIBUTIONS

Conceptualization: J.H., Methodology and Investigation: J.H., Demonstration: J.H., A.K.H., Visualization: J.H., Supervision: M.R.C., Z.B., Writing—original draft: J.H., Writing—review & editing: J.H., A.K.H., M.R.C., Z.B. The work was done at Stanford University.

COMPETING INTERESTS

The authors declare no competing interests.

ADDITIONAL INFORMATION

Supplementary information The online version contains supplementary material available at https://doi.org/10.1038/s41528-022-00225-0.

Correspondence and requests for materials should be addressed to Zhenan Bao.

Reprints and permission information is available at http://www.nature.com/reprints

Publisher's note Springer Nature remains neutral with regard to jurisdictional claims in published maps and institutional affiliations.